

# Journal of Biomedical Optics

[SPIEDigitalLibrary.org/jbo](http://SPIEDigitalLibrary.org/jbo)

## **High-throughput fabrication of gray-level biomicrostructures via temporal focusing excitation and laser pulse control**

Yi-Cheng Li  
Li-Chung Cheng  
Chia-Yuan Chang  
Chun-Yu Lin  
Nan-Shan Chang  
Paul J. Campagnola  
Chen Yuan Dong  
Shean-Jen Chen

# High-throughput fabrication of gray-level biomicrostructures via temporal focusing excitation and laser pulse control

Yi-Cheng Li,<sup>a</sup> Li-Chung Cheng,<sup>a</sup> Chia-Yuan Chang,<sup>a</sup> Chun-Yu Lin,<sup>b</sup> Nan-Shan Chang,<sup>b</sup> Paul J. Campagnola,<sup>c</sup> Chen Yuan Dong,<sup>d</sup> and Shean-Jen Chen<sup>e,f,g</sup>

<sup>a</sup>National Cheng Kung University, Department of Photonics, Tainan 701, Taiwan

<sup>b</sup>National Cheng Kung University, Institute of Molecular Medicine, Tainan 701, Taiwan

<sup>c</sup>University of Wisconsin–Madison, Department of Biomedical Engineering, Madison, Wisconsin 53706

<sup>d</sup>National Taiwan University, Department of Physics, Taipei 106, Taiwan

<sup>e</sup>National Cheng Kung University, Department of Engineering Science, Tainan 701, Taiwan

<sup>f</sup>National Cheng Kung University, Advanced Optoelectronic Technology Center, Tainan 701, Taiwan

<sup>g</sup>National Cheng Kung University, Center for Micro/Nano Science and Technology, Tainan 701, Taiwan

**Abstract.** A developed temporal focusing-based multiphoton excitation system with additional patterned excitation and local laser control can provide high-throughput fabrication of three-dimensional gray-level biomicrostructures via two-photon cross-linking with rose bengal (RB) as the photoactivator. Multiple bovine serum albumin (BSA) structures of different concentrations were simultaneously achieved by selecting different pulse numbers in the designated regions with an appropriate femtosecond laser power within a few seconds. Intensity of the RB two-photon excited fluorescence (TPEF) is correlated to the concentration of the fabricated cross-linked BSA microstructure. Hence, the fabricated BSA microstructure can be monitored online by utilizing the RB TPEF as contrast agent. It suggests that this approach with its unique capability of high-speed, gray-level, and online-inspection fabrication meets the requirements of the biomedical researches involved in extracellular matrix. © 2013 Society of Photo-Optical Instrumentation Engineers (SPIE) [DOI: 10.1117/1.JBO.18.7.075004]

Keywords: multiphoton excitation; high throughput; microfabrication; temporal focusing; biomicrostructures.

Paper 130195RR received Apr. 2, 2013; revised manuscript received Jun. 6, 2013; accepted for publication Jun. 28, 2013; published online Jul. 25, 2013.

## 1 Introduction

Photopolymerization or photo-cross-linking is a process combining light with a low-molecular-weight photoinitiator to trigger the polymerization or cross-linking reaction.<sup>1–3</sup> To fabricate three-dimensional (3-D) microstructures with specific 3-D sub-micron features, single-photon<sup>4,5</sup> and multiphoton<sup>6,7</sup> excited (MPE) photochemistry can be used.<sup>8,9</sup> Nevertheless, multiphoton absorption is more confined to the focal volume for delivering finer and taller structures. However, the major drawback of the approaches is the point-scanning process, which slows fabrication speed. Although using self-assembly of colloidal spheres is workable for the mass-production of photonics crystals,<sup>10</sup> it is limited to periodic structures. Other methods such as glancing angle deposition and the combination of nanolithography with alternating-layer deposition can further enhance the complexity of structures.<sup>11,12</sup> However, the fabrication of large-scale freeform microstructures still cannot be achieved. Although another interference method, namely holographic lithography, can make nonperiodic structures,<sup>13</sup> to obtain the desired intensity pattern, calculation of the phase information is needed in advance. In response, recent studies have shown that combining spatial and temporal focusing techniques can provide wide-field and axially resolved MPE.<sup>14–18</sup> Temporal focusing uses a diffraction grating to separate frequencies spatially and then recombines them on the focal plane of an

objective lens. Therefore, the different frequency components overlap in phase only in that plane and produce a short, high-peak power pulse, allowing MPE to occur over an entire area at one time. This provides a solution to the above drawback and enables high-throughput freeform manufacturing.

Previously, this temporal focusing setup was successfully developed to realize patterned excitation with sufficient instantaneous peak power.<sup>19</sup> By adjusting the femtosecond laser power, 3-D polymer microstructures can be fabricated within a few seconds via two-photon polymerization (TPP), offering a greater than three-order increase in fabrication speed compared to conventional MPE scanning. However, resin materials fabricated via TPP are not much suitable for biomedical applications, so biocompatible microstructures for further biological research are required. It is now well-known that spatial concentration gradients (i.e., gray level) of bioactive molecules in the extracellular matrix (ECM) play important roles in several areas of cell biology, including morphogenesis, wound healing, and metastasis.<sup>20–22</sup> Several novel optical schemes improving upon this limitation by using photochemical approaches to covalently link protein molecules to surfaces have been reported. To yield even greater versatility, fabricating covalently linked gradients directly from native ECM proteins without the need for preliminary synthetic steps would be advantageous. Hence, how to fabricate large-scale freeform gray-level protein structures should be a big issue for the biomedical researches involved in ECM.

Address all correspondence to: Shean-Jen Chen, National Cheng Kung University, Department of Engineering Science, Tainan 701, Taiwan. Tel: +886-6-2757575 ext. 63351; Fax: +886-6-2766549; E-mail: sheanjen@mail.ncku.edu.tw

0091-3286/2013/\$25.00 © 2013 SPIE

In this study, we present a new approach to quickly fabricate 3-D covalently linked protein gray-level microstructures through the use of MPE photochemistry based on temporal focusing excitation. 3-D gray-level bovine serum albumin (BSA) microstructures were fabricated by two-photon cross-linking (TPC) using rose bengal (RB) as the photoactivator. Compared to TPP, a TPC biomicrostructure is more difficult to achieve by only controlling the average fabrication power; herein, another approach controlling the pulse number of the laser is adopted. To this end, the gated-mode operation of the ultrafast amplifier and the gray-level adjustment of the digital micromirror device (DMD) were both utilized to select the pulse number. Under the gated-mode operation, a LabVIEW program was synchronized with the amplifier so that the overall pulse number per layer could be controlled. In addition, 0 to 255 gray levels represent different “on” state times for the 8-bit DMD, meaning that the DMD can act as a pulse selector to tune the laser pulse on or off, and further adjust the pulse number locally. Via the above mechanisms, gray-level BSA microstructures with different concentrations can be achieved based on the overall and local control of the femtosecond laser pulse number. Moreover, RB two-photon excited fluorescence (TPEF) can be used as contrast agent.<sup>23,24</sup> Therefore, online 3-D inspection of the fabricated BSA microstructures without washing out the unreacted solution can be offered. A 3-D multiobject BSA microstructure with three different concentrations was fabricated simultaneously within a few seconds and monitored on line by the developed multiphoton microfabrication system.

## 2 Sample Preparation and Microfabrication Setup

### 2.1 High-Throughput MPE Microfabrication System

The temporal focusing-based high-throughput multiphoton microfabrication system with patterned excitation and pulse selection developed in this study is similar to that in our previous study.<sup>19</sup> Key components include a titanium-sapphire (Ti-Sa) ultrafast amplifier, an ultrafast oscillator as the seed beam, an upright optical microscope, a triple-axis sample positioning stage, an Andor electron multiplying charge-coupled device camera, a DMD, and a data acquisition card with a field-programmable gate array (FPGA) module. The ultrafast amplifier has a maximum peak power of 400  $\mu$ J/pulse and a pulse width of 100 fs at an average power of 4.0 W with a repetition rate of 10 kHz. The DMD chip, controlled by a digital light processing technique, generates the designed fabrication pattern. The motorized stage is controlled in the  $z$  axis via the FPGA, allowing sequential and variable depth two-dimensional (2-D) patterned MPE fabrication to be quickly realized. In addition, the system features both bright-field and wide-field MPE fluorescence optics, acquiring either white light or TPEF images during the fabrication process for online diagnostics of the fabricated structures.

One issue affecting the system is the group velocity dispersion of the ultrafast amplifier due to the objective lens, collimating lenses, and other refractive elements. To rectify this, the amplifier's built-in prism pair can be adjusted to the optimal pulse width (<120 fs) according to a developed Michelson-interferometry-based autocorrelator to measure the pulse width of the amplifier on the sample surface.<sup>15</sup> Consequently, the temporal focusing efficiency for MPE polymerization or cross-linking can be enhanced, allowing faster multiphoton microfabrication. Compared to holographic

femtosecond laser processing,<sup>13,25</sup> this system not only accurately fabricates 3-D microstructures but also provides optical sectioning on line. Although patterned excitation via the DMD fabricates the microstructures, uniform excitation images the fabricated microstructures when all pixels in the DMD are activated. Accordingly, if the TPEF contrast between the remaining solution and the fabricated microstructures is sufficiently high,<sup>23</sup> direct observation of the microstructures' production without removing the fabrication solution or additional follow-up imaging can be achieved.

### 2.2 Designing 3-D Freeform Structures and Biomonomer Preparation

The creation of any solid 3-D freeform microstructure based on this microfabrication configuration can be accomplished using commercial CAD software such as AutoCAD, Pro/E, and Solidworks. 3-D structures can be transformed into 2-D processing patterns by initially converting the 3-D models into stereolithography (STL) format and saving them as output files. The STL files are then read by our LabVIEW program and converted into sequential 2-D BMP files. Finally, the converted BMP files are read by another LabVIEW program that sequentially displays the sliced BMP patterns on a processing monitor. The DMD then synchronizes with the display patterns and generates patterned excitation on the focal plane of the objective lens, thereby creating specified structures.

A protein, BSA (Sigma-Aldrich, USA), was employed as the reactive monomer with RB incorporated (Avocado Research Chemicals, UK) as the photoactivator in the fabrication solution. All chemicals and reagents were of analytical grade. According to our previous point-scanning MPE experimental results, 20 mg/ml of BSA solution with  $\sim$ 2.0 mM RB is appropriate. Herein, the high-throughput microfabrication is a collective reaction, so the BSA in the fabricated solution and the RB concentration were increased to 150 mg/ml and 20 mM, respectively. Then, 30  $\mu$ l of fabrication solution was confined in a small chamber created using a 40- $\mu$ m-thick adhesive tape as a spacer to separate a 0.17 mm cover slip and the microscope slide. During fabrication, structures were created from the bottom (slide) to the top (slip) to prevent the incoming patterned excitation from being distorted by previously developed microstructures. According to our previous experiment,<sup>26</sup> the two-photon absorption peak of RB is around 715 nm; nevertheless, the range of the Ti-Sa ultrafast amplifier can be adjusted from 750 to 850 nm. The shortest laser wavelength of 750 nm was adopted and is sufficient for the TPC process.

## 3 Experimental Results and Discussions

### 3.1 System Calibrations for Fabricating BSA Microstructures

Based on our experimental experience, control of the laser peak power and pulse number is a key parameter due to the efficiency limits of the TPC process. If the peak power is too low, MPE photochemistry in wide-field excitation cannot be achieved; on the other hand, if the peak power of a single pulse is too high, damage to biosamples such as BSA, might occur within only a few pulses. The laser peak power of the Ti-Sa ultrafast amplifier is difficult to control evenly and precisely; hence, a suitable peak power level was initially chosen, and then the pulse number was controlled to accumulate an appropriate dose. Two

mechanisms are implemented for precisely accumulating the global and local doses in the high-throughput MPE system, namely the gated-mode operation of the amplifier system and the DMD chip, respectively. Under gated-mode operation, our LabVIEW program synchronizes with the amplifier system; hence, the global pulse number of the laser incident on the sample per layer can be selected. For an 8-bit DMD, the 0 to 255 gray levels represent different “on” state times, which means that it can act as a pulse selector to tune the laser pulse optional on or off in the fabrication area. In other words, the DMD gray level acts as an optical shutter that adjusts the local pulse number at every layer. For example, for an amplifier repetition rate of 10 kHz, a gray level of 255 represents 10,000 pulses per second, while a gray level of 128 refers to 5000 pulses per second, and so on. Under the gated-mode operation, the relationship between the normalized TPEF intensity and the laser pulse number at the fluence of  $35 \mu\text{J}/\text{pulse}$  is presented in Fig. 1(a). The correlation is approximately linear and nearly matches theoretical predictions. Figure 1(b) illustrates the TPEF intensity as a function of different DMD gray levels, with the gated-mode operation controlling the global pulse number at 1000 and where the fluence of each pulse is also  $35 \mu\text{J}$ . Again, the relation is almost linear, thus providing further evidence that the DMD can reliably act as a second pulse selector to locally control the pulse number. Based on the two figures, our strategy for fabricating 3-D gray-level BSA microstructures employs the gated-mode operation to initially decide the global pulse number and then locally assigns the pulse number via the gray-level DMD.

With the global and local pulse number selectors, the lateral resolution for fabricating cross-linked BSA structures requires clarification for further processing. According to the current adjusted magnification of the system, a fabrication area of  $76 \times 43 \mu\text{m}^2$  corresponds to the  $640 \times 360$  pixel number of the DMD chip, indicating that 1 pixel corresponds to roughly  $120 \times 120 \text{ nm}^2$  on the sample. Three stripe patterns with pixel numbers of 46, 23, and 14, with respective corresponding widths of around 5.5, 2.7, and  $1.6 \mu\text{m}$ , were designed to examine the lateral resolution. However, since the beam profile is a Gaussian distribution and BSA photo-cross-linking requires a threshold fabrication energy to initiate the TPC process, the actual fabricated sizes are smaller than the designed sizes. Figure 2(a) and 2(b) show that the fabricated widths of the stripes are  $\sim 2.3$  and  $1.1 \mu\text{m}$ , which correspond to the designed

widths of 5.5 and  $2.7 \mu\text{m}$ , respectively. Experimental results indicate that both widths of the fabricated stripes are reduced  $\sim 60\%$ . However, the fabricated width of the smallest stripe corresponding to the designed size of  $1.6 \mu\text{m}$  is also around  $1.1 \mu\text{m}$  (data not shown here), which may result from the diffraction limit and/or system distortion. Consequently, the lateral fabrication resolution of the current system is around  $1 \mu\text{m}$ .

The potential to separate layers vertically is dependent on the axial fabrication resolution of the system. According to our previous study,<sup>27</sup> an axial imaging resolution of  $<3.4 \mu\text{m}$  can be provided as the maximum laser power is  $<40 \text{ mW}$ . For fabrication, the TPP and TPC processes use photoinitiators to trigger reactions, so an optical energy threshold to initiate the process is required, which can lead to the axial fabrication resolution being better than that of the imaging. Furthermore, the axial fabrication resolution is related to the material used; hence, an axial fabrication resolution of  $<2 \mu\text{m}$  can be achieved for BSA structures in the current system. Besides having the pulse selecting capability, the DMD can further enhance the axial resolution of the system. In the original temporal focusing setup, the pulsing beam is spatially dispersed via a grating in the meridian plane; then the spatially dispersed frequencies go through a  $4f$  setup to realize temporal focusing excitation. Due to this setup, the beam is focused as a line on the back-focal plane of the objective lens. The incorporation of the DMD into the system can also function as a grating. Therefore, the different frequencies of the pulsing beam can be spatially dispersed again in the sagittal plane. Consequently, the width of the line becomes wider on the back-focal plane. On increasing the beam coverage area on the back-focal plane, a larger numerical aperture (NA) of the system is utilized. Therefore, the axial resolution is improved. Moreover, the higher the chosen order of the DMD diffraction pattern, the larger the NA that is utilized.

### 3.2 Online Imaging of Cross-Linked BSA Microstructures

As mentioned above, this system not only fabricates 3-D free-form microstructures but also provides fast optical sectioning. According to our previous study on BSA microstructures, the RB TPEF contrast between the fabricated microstructures and the remaining BSA solution is sufficiently high to allow for immediate inspection of the fabricated microstructures without removing unreacted solution or additional follow-up imaging.

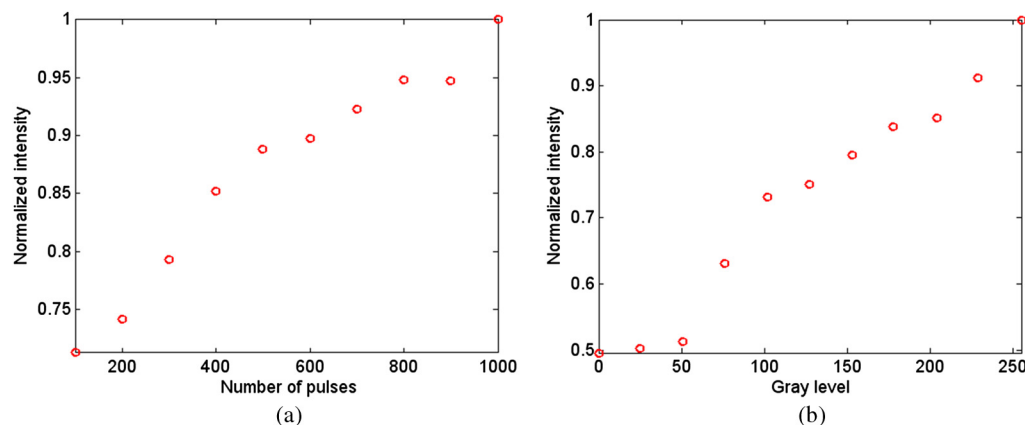


**Fig. 1** (a) Normalized TPEF intensity as a function of different pulse number under the gated-mode operation. Fluence of each pulse is  $35 \mu\text{J}$ . (b) Relationship between the normalized TPEF intensity and the DMD gray level with gated-mode operation to control the global pulse number of 1000.

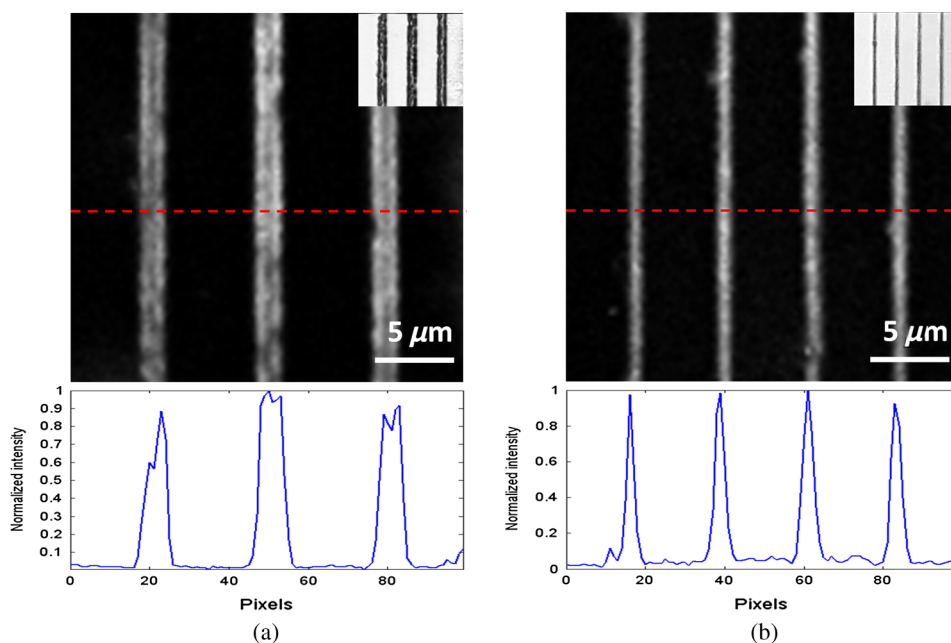


**Fig. 2** TPEF images and profiles of two stripes fabricated with the pixel numbers of (a) 46 and (b) 23, the fabricated widths of which are 2.3 and 1.1  $\mu\text{m}$ , respectively. The profiles correspond to the red dash line in the TPEF images. Inset: corresponding 2-D front-view bright-field images.

Figure 3 illustrates four different structures that were fabricated simultaneously, the heights of which are 15  $\mu\text{m}$ . The fabrication parameters are 1000 pulses per layer with a fluence of 35  $\mu\text{J}$  per pulse and a  $z$  axis step of 0.5  $\mu\text{m}$ . A fabrication time of only 3 s demonstrates that fabrication speed is at least 1000 times as fast as conventional point-scanning microfabrication. Herein, the throughput depends on the magnification of the system. The throughput of volume-per-time is around 16,340  $\mu\text{m}^3/\text{s}$  under a fabrication area of  $76 \times 43 \mu\text{m}^2$  with a 40 $\times$  objective lens, where the  $z$  axis step is 0.5  $\mu\text{m}$  and the fabrication time per layer is  $\sim 0.1$  s. When a 20 $\times$  objective lens is adopted, fabrication can be increased to 65,360  $\mu\text{m}^3/\text{s}$ , and so on. The throughput can be further improved via readjusting the magnification of the relay lens pairs in the system setup. Furthermore, the Gaussian beam scan is a point-by-point process; however, spatiotemporal focusing uses a 4 $f$  setup to realize wide-field excitation. Therefore, the cross-linking process is a collective response, not an individual one, which means that adjacent biomolecules may interact with one another. If the size of the fabrication pattern is large, we can simply use a relatively lower

laser dose per unit area to deliver the structure. By contrast, if the size is small, then fewer molecules are inside the fabrication area and a relatively larger laser dose per unit area is needed. Based on our experimental experience under this setup, the laser dose required for TPC depends on the size that one wishes to fabricate.

As can be seen, the TPEF intensity of the fabricated structures is higher than that of the remaining solution; therefore, non-patterned excitation can be utilized for online inspection of the fabricated BSA structures, as Fig. 3(a) shows. Figure 3(b) offers the TPEF images of these structures using point-scanning microscopy after washing out the unreacted solution; however, a refractive index mismatch occurs between the BSA structures and air, leading to aberrations and distortions. Consequently, the TPEF intensity is not uniform and image quality is poor. To correct this issue, match oil was introduced into the sample chamber to produce a better TPEF image, as Fig. 3(c) demonstrates. Figure 3(a) image appears slightly blurry compared to that of Fig. 3(c) due to the background noise from the remaining solution; however, the online inspection via this high-throughput

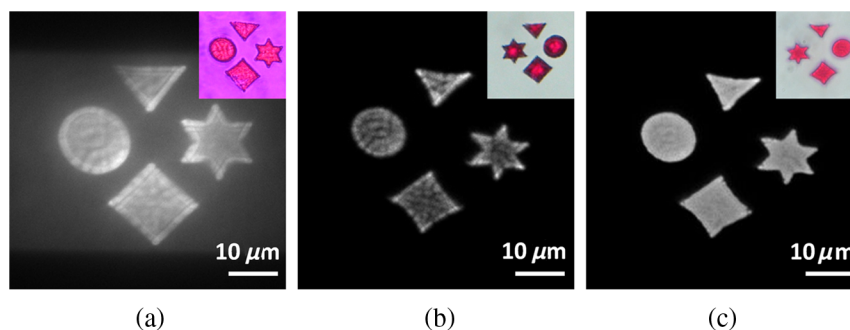


**Fig. 3** TPEF images of the fabricated multiobject BSA microstructures. (a) Wide-field imaging before washing out the remaining solution. (b) Image acquired via conventional point-scanning microscopy after washing out the remaining solution. (c) Image of (b) acquired after adding match oil. Inset: corresponding 2-D front-view bright-field images. Videos 1 and 2 are the 3-D renderings of (b) and (c), respectively (Video 1, QuickTime, 353 KB [URL: <http://dx.doi.org/10.1117/1.JBO.18.7.075004.1>]; Video 2, QuickTime, 407 KB [URL: <http://dx.doi.org/10.1117/1.JBO.18.7.075004.2>]).

multiphoton lithography system can provide online quality monitoring of the fabricated microstructures without additional follow-up processes. Furthermore, based on our previous study,<sup>22</sup> the heights of fabricated BSA microstructures can exceed 100  $\mu\text{m}$ , but are not workable for laminin and fibronectin. Although an imaging depth of 100  $\mu\text{m}$  for BSA microstructures via the wide-field system can be achieved, if the material is more transparent, the penetration depth can be deepened.

### 3.3 Fabrication of 3-D Gray-Level BSA Microstructures

According to our study, the RB TPEF intensity in the fabricated cross-linked BSA microstructures was strongly related to the laser dose under the same BSA solution. By raising the laser dose, the concentration of the cross-linked BSA microstructure can be increased, which in turn can enlarge the TPEF quantum yield of RB. This indicates that the gray-level degrees (i.e., concentrations) within the fabricated BSA structures can be examined via the RB TPEF intensities. Under the multiphoton microfabrication system, concentrations of the fabricated BSA microstructures can be easily manipulated by globally and locally selecting the pulse numbers under the same laser power and BSA solution concentration. Figure 4(a) shows a designed pattern of  $2 \times 3$  squares (each square measures  $12 \times 12 \mu\text{m}^2$ ) simultaneously fabricated as BSA microsquares at the fluence of  $35 \mu\text{J}$  per pulse and a BSA solution concentration of 150 mg/ml under different pulse selections. The global pulse number was fixed at 1000 pulses via the gated-mode operation, and the localized

gray levels of the squares were altered with a sequentially decreasing interval of around 25 via the DMD chip, from an initial 255 (1000 pulses) at the upper left-hand corner down to 127 (500 pulses) at the lower right-hand corner. Figure 4(b) shows that the designed BSA microstructures are completely fabricated at a gray level  $>153$ , while the RB TPEF intensity gradually weakens with reduced gray levels (i.e., relatively lower pulse numbers). Figure 4(c) demonstrates the relative TPEF intensity profile of the cross-linked BSA microstructures indicated by the red dash line in Fig. 4(b). Based on our study, the TPEF intensity increase of a higher gray-level BSA structure is due to its enlarged TPEF quantum yield and shortened lifetime via a higher concentration BSA structure and higher fabrication laser dose.

According to the above experiments, 3-D BSA cross-linked microstructures with different local concentrations can be fabricated using the pulse selectors at fully developed laser fluence. To demonstrate the capability of developing freeform 3-D gray-level BSA microstructures, three different patterns with varying gray levels were fabricated. Based on the results given in Fig. 4, a square, circle, and triangle with respective gray levels of 255, 204, and 153 under the maximum pulse number of 1000 pulses per layer were fabricated. This indicates that pulse numbers of 1000, 800, and 600 correspond to the square, circle, and triangle, respectively. The total number of layers was 30, while the  $z$  axis step was 0.5  $\mu\text{m}$ . Thus, the microstructures' fabrication time was only 3 s. Figure 5(a) is the TPEF image of the fabricated 3-D gray-level multiobject BSA microstructures before cleansing the remaining solution. Although the contrast is not perfect, it can be seen that the intensity of the square is the

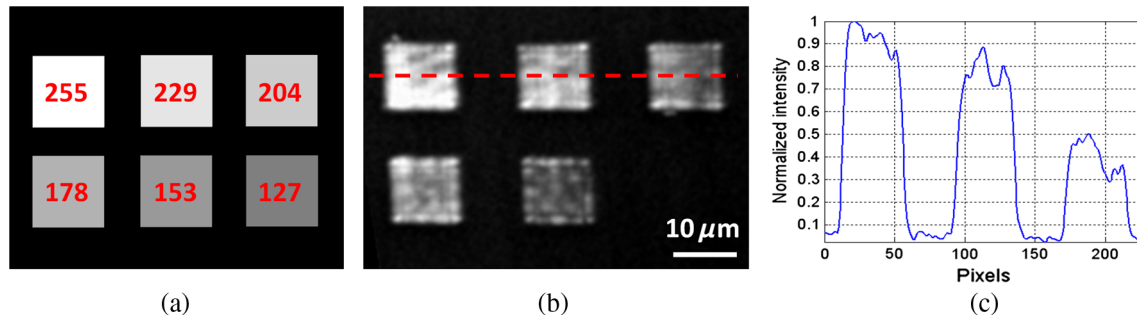


**Fig. 4** Images and profile of the RB TPEF intensity in the cross-linked BSA microstructures fabricated by globally and locally selecting the pulse numbers. (a) Designed gray-level pattern of  $2 \times 3$  squares (each square measures  $12 \times 12 \mu\text{m}^2$ ) from the highest level of 255 to the lowest level of 127 via the DMD. (b) The corresponding TPEF image of the fabricated gray-level BSA microsquares. (c) Profile corresponding to the red dash line in (b).

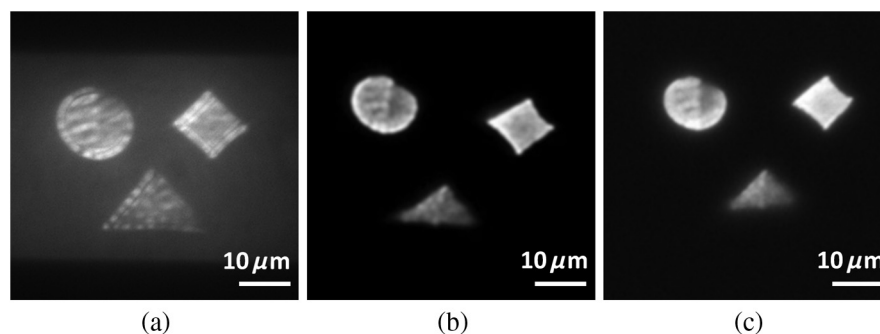


**Fig. 5** TPEF images of the fabricated gray-level multiobject BSA microstructures via (a) the multiphoton lithography system before cleansing the remaining solution, and (b) the conventional point-scanning multiphoton microscope and (c) the multiphoton lithography system, both after washing out the unreacted solution and injecting match oil. Videos 3 and 4 are the 3-D renderings of (b) and (c), respectively (Video 3, QuickTime, 289 KB [URL: <http://dx.doi.org/10.1117/1.JBO.18.7.075004.3>]; Video 4, QuickTime, 261 KB [URL: <http://dx.doi.org/10.1117/1.JBO.18.7.075004.4>]).

highest while that of the triangle the lowest. Figure 5(b) presents the TPEF images captured by a conventional point-scanning microscope after cleansing the remaining solution and injecting match oil. The contrast of the TPEF image is high and confirms that multiple freeform 3-D microstructures with different gray levels (i.e., local concentrations) can be achieved within a few seconds. The gray-level BSA microstructures with added match oil were imaged again using the multiphoton lithography system, as shown in Fig. 5(c), which displays an image quality comparable to that of Fig. 5(b). According to our previous study,<sup>27</sup> an image lateral resolution >500 nm can be achieved with this system.

## 4 Conclusions

In this study, a developed temporal focusing-based multiphoton excitation system with additional patterned excitation and laser pulse control was utilized to quickly fabricate 3-D gray-level BSA microstructures via TPC processing. A wide dynamic range in the BSA microstructures' concentration was achieved based on globally and locally selecting the pulse number via the gated-mode operation and the gray level of the DMD chip, respectively. Furthermore, this system offers optical sectioning for 3-D online inspection of the fabricated microstructure by utilizing the RB TPEF as contrast agent. 3-D multiobject BSA microstructures with different gray levels were simultaneously fabricated and monitored on line within a few seconds. 3-D protein concentration gradients can act as a structured biomaterial for tissue engineering; hence, this approach with its unique capability of high-speed, gray-level, and online-inspection fabrication may render ECM more popular for biomedical research.

## Acknowledgments

Chun-Yu Lin and Nan-Shan Chang (NSC) acknowledge support from NSC 100-2811-B-006-035. Paul J. Campagnola acknowledges support from NSF CBET-1057766. Shean-Jen Chen acknowledges support from NSC 101-2221-E-006-212-MY3 and NSC 101-2221-E-006-213-MY3.

## References

1. C. R. Lambert, I. E. Kochevar, and R. W. Redmond, "Differential reactivity of upper triplet states produces wavelength-dependent two-photon photosensitization using rose bengal," *J. Phys. Chem. B* **103**(18), 3737–3741 (1999).
2. J. D. Pitts et al., "Submicron multiphoton free-form fabrication of proteins and polymers: studies of reaction efficiencies and applications in sustained release," *Macromolecules* **33**(5), 1514–1523 (2000).
3. P. J. Campagnola et al., "3-dimensional submicron polymerization of acrylamide by multiphoton excitation of xanthene dyes," *Macromolecules* **33**(5), 1511–1513 (2000).
4. S. Maruo and K. Ikuta, "Three-dimensional microfabrication by use of single-photon-absorbed polymerization," *Appl. Phys. Lett.* **76**(19), 2656–2658 (2000).
5. M. Thiel et al., "Direct laser writing of three-dimensional submicron structures using a continuous-wave laser at 532 nm," *Appl. Phys. Lett.* **97**(22), 221102 (2010).
6. S. Kawata et al., "Finer features for functional microdevices," *Nature* **412**(6848), 697–698 (2001).
7. W. Denk, J. H. Strickler, and W. W. Webb, "Two-photon laser scanning fluorescence microscopy," *Science* **248**(4951), 73–76 (1990).
8. M. Malinauskas et al., "Mechanisms of three-dimensional structuring of photo-polymers by tightly focused femtosecond laser pulses," *Opt. Express* **18**(10), 10209–10221 (2010).
9. M. Malinauskas, P. Danilevicius, and S. Juodkazis, "Three-dimensional micro-/nano-structuring via direct write polymerization with picosecond laser pulses," *Opt. Express* **19**(6), 5602–5610 (2011).
10. Y. A. Vlasov et al., "On-chip natural assembly of silicon photonic bandgap crystals," *Nature* **414**(6861), 289–293 (2001).
11. S. R. Kennedy et al., "Fabrication of tetragonal square spiral photonic crystals," *Nano Lett.* **2**(1), 59–62 (2002).
12. E. Kuramochi et al., "A new fabrication technique for photonic crystals: nanolithography combined with alternating-layer deposition," *Opt. Quant. Elec.* **34**(1–3), 53–61 (2002).
13. D. N. Sharp et al., "Photonic crystals for the visible spectrum by holographic lithography," *Opt. Quant. Elec.* **34**(1–3), 3–12 (2002).
14. D. Oron, E. Tal, and Y. Silberberg, "Scanningless depth-resolved microscopy," *Opt. Express* **13**(5), 1468–1476 (2005).
15. G. Zhu et al., "Simultaneous spatial and temporal focusing of femtosecond pulses," *Opt. Express* **13**(6), 2153–2159 (2005).
16. J. Vaziri et al., "Multilayer three-dimensional super resolution imaging of thick biological samples," *PNAS* **105**(51), 20221–20226 (2008).
17. E. Papagiakoumou et al., "Scanless two-photon excitation of channelrhodopsin-2," *Nat. Methods* **7**(10), 848–854 (2010).
18. D. Therrien et al., "Wide-field multiphoton imaging of cellular dynamics in thick tissue by temporal focusing and patterned illumination," *Biomed. Opt. Express* **2**(3), 696–704 (2011).
19. Y.-C. Li et al., "Fast multiphoton microfabrication of freeform polymer microstructures by spatiotemporal focusing and patterned excitation," *Opt. Express* **20**(17), 19030–19038 (2012).
20. M. A. Swartz, "Signaling in morphogenesis: transport cues in morphogenesis," *Curr. Opin. Biotechnol.* **14**(5), 547–550 (2003).
21. L. Liaw et al., "Adhesive and migratory effects of osteopontin are mediated via distinct cell-surface integrins—Role of alpha v beta 3 in smooth-muscle cell-migration to osteopontin in-vitro," *J. Clin. Invest.* **95**(2), 713–724 (1995).
22. X. Chen et al., "Cell adhesion on micro-structured fibronectin gradients fabricated by multiphoton excited photochemistry," *Cell. Mol. Bioeng.* **5**(3), 307–319 (2012).
23. K.-C. Cho et al., "Enhanced two-photon excited fluorescence in three-dimensionally crosslinked bovine serum albumin microstructures," *Opt. Express* **19**(12), 11732–11739 (2011).
24. C.-Y. Lin et al., "Investigation of two-photon excited fluorescence increment via crosslinked bovine serum albumin," *Opt. Express* **20**(13), 13669–13676 (2012).
25. S. Hasegawa and Y. Hayasaki, "Adaptive optimization of hologram in holographic femtosecond laser processing system," *Opt. Lett.* **34**(1), 22–24 (2009).
26. W. S. Kuo et al., "Multiphoton fabrication of freeform polymer microstructures with gold nanorods," *Opt. Express* **18**(26), 27550–27559 (2010).
27. L.-C. Cheng et al., "Spatiotemporal focusing-based widefield multiphoton microscopy for fast optical sectioning," *Opt. Express* **20**(8), 8939–8948 (2012).